

Thresholds and the role of the radial electric field in confinement bifurcations in the H-1 heliac

M. G. Shats,^{a)} C. A. Michael, D. L. Rudakov, and B. D. Blackwell

Plasma Research Laboratory, Research School of Physical Sciences and Engineering, Australian National University, Canberra 0200, Australia

(Received 25 November 1997; accepted 17 March 1998)

The threshold conditions for the confinement bifurcations in the H-1 heliac [S. M. Hamberger *et al.*, *Fusion Technol.* **17**, 123 (1990)] are studied experimentally. The thresholds include the magnetic field, the rf power, and the neutral gas filling pressure. It is shown that in any combination of these parameters it is the radial electric field E_r that is driven to a critical value before the bifurcation. A mechanism of the electric field formation is suggested, which is based on the balance of the electron and ion losses. The ion loss, at low magnetic field and high ion temperature observed in H-1, is dominated by the direct orbit loss mechanism. This is shown by modeling of the exact ion orbits and by comparing a qualitative picture of the E_r formation with the experimental data. Relative efficiency of the electron and ion heating in the inner regions of plasma define the conditions for either low-to-high (L-H) or high-to low (H-L) confinement bifurcations in H-1. © 1998 American Institute of Physics. [S1070-664X(98)03706-9]

I. INTRODUCTION

The radial electric field has been shown to play a crucial role in the confinement of plasmas in toroidal machines.¹ It is also a major player in confinement bifurcations observed in tokamaks,² stellarators,³⁻⁵ reversed-field pinch configurations⁶ and in linear machines.⁷

The transitions to improved confinement modes observed in the H-1 toroidal heliac⁸⁻¹⁰ exhibit many of the features of low-to-high (L-H) transitions in other experiments, including the increase in the radial electric field across the transition from low (L) to high (H) confinement mode. Whether such an increase causes the transition, or it is a result of the improvement in confinement (because of the steeper ion pressure gradients in the H mode) is not quite clear. This question is closely related to a practical problem of the thresholds for the transitions (see, for example, Ref. 11): which plasma parameters define the conditions favorable for the confinement bifurcations.

In this paper we present the experimental results on the thresholds for the L-H transitions in the H-1 heliac and analyze the role of the radial electric field E_r in bringing the plasma up to a bifurcation point. The experimental setup and diagnostics used in this study are described in Sec. II. The experimental results on the transition thresholds and on the E_r behavior are presented in Sec. III. It is shown that in any combination of the plasma parameters (magnetic field, rf power, neutral pressure, etc.) it is the E_r that needs to be driven to a certain critical value. At this point, we postulate that driving E_r above the critical is a necessary condition for a bifurcation. The next question is *how* does the plasma approach a bifurcation?

Though the transitions between the confinement modes in H-1 are similar in many aspects to those in other ma-

chines, the physics can be quite different, for the following reasons. The transitions are observed at a very low magnetic field (<0.15 T), low electron temperature (<30 eV), and surprisingly high ion temperature (up to 200 eV). The transitions are observed in argon, neon, helium, and hydrogen plasmas. A very large ion gyroradius ($\sim 6-10$ cm in a high T_i argon plasma), comparable to the minor plasma radius, implies that the ion transport phenomena cannot be described by the existing theories, since a $\rho_{Li}/L_n \ll 1$ ordering (where ρ_{Li} is the ion Larmor radius and L_n is the density scale length) used in most of the neoclassical approaches is not applicable to our conditions. The main ion loss mechanism is the direct ion orbit loss. The electrons, on the other hand, are strongly magnetized ($\rho_{Le} \sim 0.1$ mm), so that the electron transport is diffusive. In this paper we study the plasma particle loss using a three-dimensional (3-D) ion orbit modeling to analyze its role in bringing E_r to a critical value.

In steady state, the quasineutrality requires that the radial fluxes of electrons and ions be equal. This equality is maintained by the radial electric field, which in the case of H-1 is negative (directed inward).⁸ We analyze the electron and ion radial fluxes, assuming the ion orbit loss to be dominant and considering the fluctuation-induced flux to be ambipolar.

In Sec. IV we present the results on the ion orbit modeling in a 3-D magnetic field in the presence of the radial electric field. The modeling results on the ion loss rate are used to derive an empirical scaling of the outward ion flux.

In Sec. V we present a simple qualitative model of the formation of the radial electric field and compare its predictions with experimental results. In Sec. VI we summarize the results.

II. EXPERIMENTAL SETUP, DIAGNOSTICS AND PLASMA PARAMETERS

The H-1 heliac is a helical axis stellarator having a major radius of $R_0 = 1.0$ m and a minor plasma radius of about 0.2

^{a)}Electronic mail: michael.shats@anu.edu.au

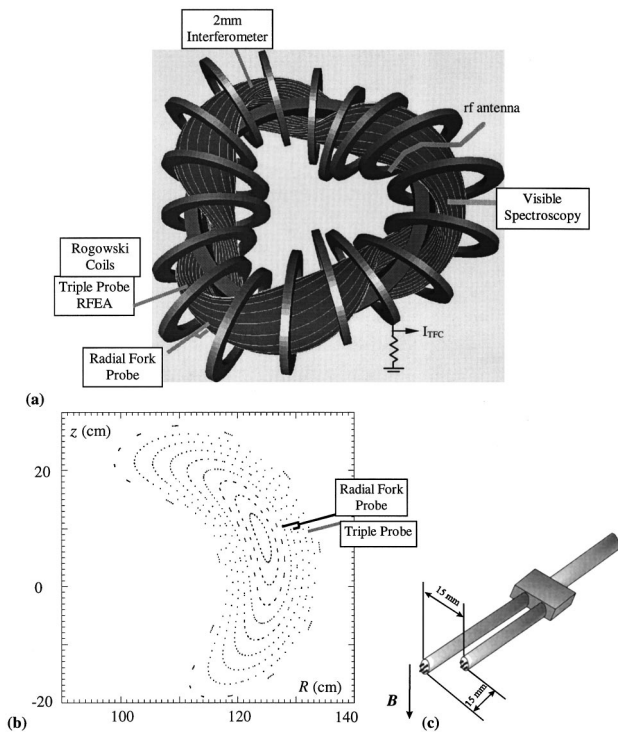


FIG. 1. The H-1 coil arrangement (half of the toroidal field coils shown) and the diagnostics location (a); the position of the triple probes in the H-1 poloidal cross-section (b). The radial fork probe [two triple probes separated as shown in (c)] is located at the toroidal angle of $\varphi = 7.5^\circ$ (tips at $r/a = 0.33$ and $r/a = 0.5$); the single triple probe is located at $\varphi = 0^\circ$ with its tips at $r/a = 1$. This fixed probe position was used in the dynamics studies.

m.¹² For the experiments reported here it was operated at low magnetic fields (< 0.2 T), with a current-free plasma produced by the pulsed rf power of less than 100 kW at 7 MHz. The rf power pulse length is about 80 ms. The electron temperature in the discharge is low enough ($T_e = 5\text{--}40$ eV) so that a number of probes can be inserted as far as the magnetic axis. The experiments are performed in argon, neon, helium, and hydrogen. The argon gives typically more reproducible discharges, which are less affected by the insertion of the probes.

The main diagnostics used in this set of experiments include the combinations of the triple probes described below, the retarding field energy analyzer (RFEA) described in Ref. 9, microwave interferometer, and a visible spectroscopy diagnostic to monitor the intensity of the chord average ion and neutral spectral lines.⁹ The diagnostic layout is shown in Fig. 1. Three triple probes capable of measuring the ion saturation current I_s , the plasma potential V_p , and the electron temperature T_e with a time resolution of about $5\ \mu\text{s}$ (limited by the acquisition rate of 200 kHz) were arranged as shown in Fig. 1(b). A single movable triple probe was typically fixed radially at about the last closed flux surface (LCFS), $r/a = 1$. This probe was located toroidally at $\varphi = 0$, while the other two triple probes were combined into a radially movable fork probe [tips separated by 15 mm both poloidally and radially, as shown in Fig. 1(c)] at $\varphi = 7.5^\circ$. This radial fork probe is used to measure a time-resolved radial electric field during a single plasma discharge. It was also used to measure

the radial electric field profiles on a shot-to-shot basis. A number of the parameter scan experiments have been performed when both the radial fork probe and the triple probe were radially fixed, measuring I_s , V_p , and T_e at $r/a = 0.33$, $r/a = 0.5$ (fork probe), and $r/a = 1.0$ (single-triple probe) simultaneously. In this case, we monitor the average gradients of the plasma potential (denoted as the average radial electric field later in the paper) and of the ion saturation current (denoted as the average density gradient). These gradients are defined as $E_r^{\text{av}} = -[V_p(r/a = 1) - V_p(r/a = 0.33)]/\Delta r$ and $dI_s/dr = [I_s(r/a = 1) - I_s(r/a = 0.33)]/\Delta r$.

The radial profiles of the plasma parameters in low and high confinement modes are described in Refs. 8 and 9. The density profiles are peaked [$n_e(0) \approx 10^{18}\ \text{m}^{-3}$], the electron temperature profiles are flat in the inner region of plasma [$T_e(0) \approx 8$ eV] increasing to the edge to about 20 eV in the L mode. In the H mode, T_e in the center remains the same or decreases to about 6 eV, while at the edge T_e increases to about 25 eV. The plasma potential is positive being $V_p \approx 30$ V in the radial region of $r/a = (0\text{--}0.5)$ and $V_p \approx 80$ V at the edge in the L mode. In the H mode, the central potential drops to $V_p \approx 5$ V while the edge plasma potential increases up to ~ 100 V. This leads to the doubling in the radial electric field in the outer half of the plasma radius across the transition from the L to the H mode. The ion temperature profile, as measured using RFEA, remains essentially flat in both modes of confinement, but the central temperature increases across the transition by up to 100% from about 40 eV in the L mode to 80 eV in the H mode.⁹ The increase in the radial electric field is not correlated with any significant changes in the ion poloidal or toroidal flows, whose velocities appear to be about five to ten times lower than the estimated $\mathbf{E} \times \mathbf{B}$ drift velocities in either mode of confinement.⁹

III. EXPERIMENTAL RESULTS ON THE TRANSITION THRESHOLDS

It has been reported in Ref. 8 that the improved confinement mode in H-1 is observed when the magnetic field is above some critical value B_{cr} . This B_{cr} changes with the rotational transform l roughly as $1/(1-l)$.⁸

First, we present the results on the transition thresholds in the magnetic configuration characterized by the rotational transform of $l \approx 1.41$ and very low shear ($\Delta l/l \approx 10^{-3}$). Among other parameters that define the conditions for the L-H transitions is the neutral particle density. Critical magnetic field B_{cr} , defined as B at which spontaneous L-H transitions are observed, increases with an increase of the filling pressure. Figure 2 shows the results of the magnetic field scan for three different filling pressures in argon at a fixed rf power. The ion saturation current at $r/a \approx 0.3$ [Fig. 2(a)] practically does not change in the L mode and increases by 60%–80% about B_{cr} . The average density gradient ($r/a = 0.33$ to 1.0) [Fig. 2(b)] does not change in the L mode and then increases at $B \approx B_{\text{cr}}$ in the H mode. The average radial electric field E_r [Fig. 2(c)] gradually increases (becomes more negative) with B in the L mode to a level of about

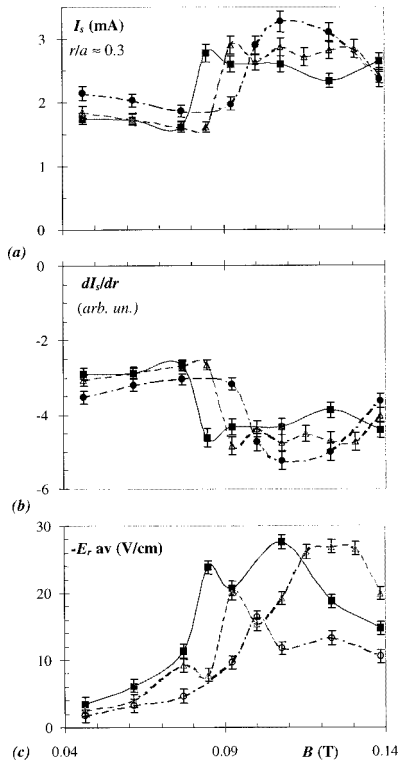


FIG. 2. Plasma parameters during the magnetic field scans: (a) ion saturation current at $r/a \approx 0.3$; (b) the radial gradient of the ion saturation current and (c) the average radial electric field at three values of the filling pressure in argon. Here $P_{fill} = 1.7 \times 10^{-5}$ Torr (squares), 2.4×10^{-5} Torr (triangles), and 3.6×10^{-5} Torr (circles). The rf power launched using two antennas is fixed at $P_{rf} \approx 80$ kW.

– 11 V/cm before it jumps up in the H mode. The error bars in Fig. 2 indicate a shot-to-shot reproducibility.

The magnetic field at which the jumps in the plasma parameters occur increases with the increase in the gas filling pressure almost linearly, as shown in Fig. 3(b). It should be noted that the ion temperature in the L mode (at a fixed magnetic field) decreases with the increase in P_{fill} , as shown in Fig. 3(a).

The rf power is another parameter that defines the thresholds for the transitions between two modes of confinement. In the magnetic configuration with $l \approx 1.41$, transitions to the H mode can be reached at a fixed magnetic field $B < B_{cr}$ and fixed filling pressure by increasing the rf power. This is illustrated in Fig. 4. As the rf power is increased from ~ 12 kW to ~ 90 kW, the line-average density stays at $n_e \sim 6 \times 10^{17} \text{ m}^{-3}$ in the L mode and then jumps up to $n_e \sim 10^{18} \text{ m}^{-3}$ in the H mode [Fig. 4(a), open squares]. Both the ion temperature [Fig. 4(b), open diamonds] and the average radial electric field [Fig. 4(a), solid circles] gradually increase with the increase in the rf power in the L mode before they suddenly double in the H mode.

The transitions to the H mode induced by the increase in the rf power are also observed in this magnetic configuration during the “power step” discharges. One example of such a discharge is shown in Fig. 5. A 17 ms long “preionization” phase is followed by four rf power steps, each ~ 15 ms long, as shown in Fig. 5(a). During the first two steps, from ~ 17

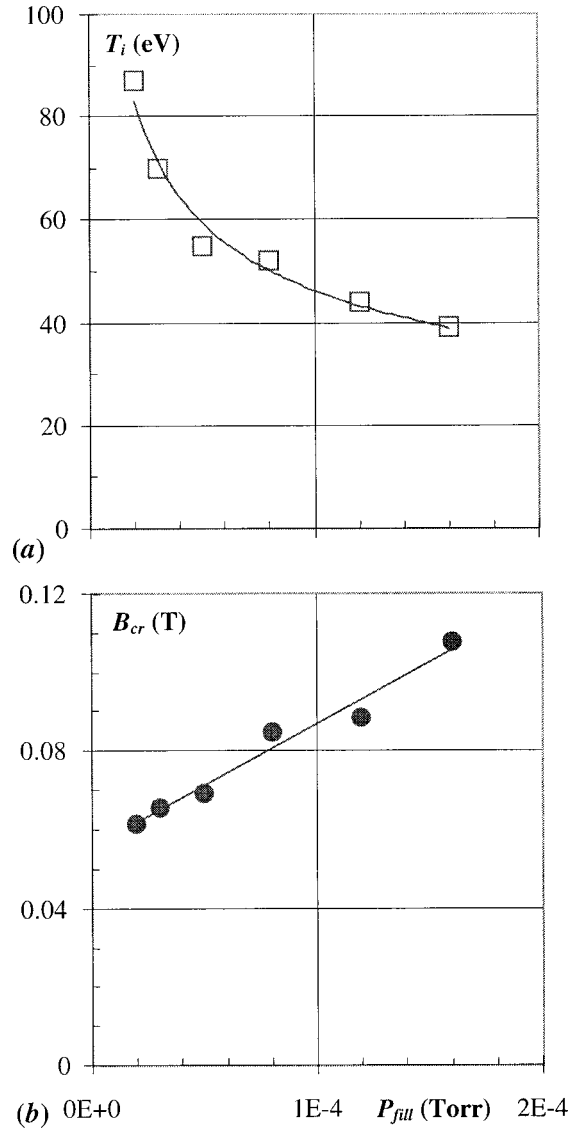


FIG. 3. The ion temperature at $r/a \approx 0.3$ in the L mode at $B = 0.06$ T, (a), and the critical magnetic field, (b), versus gas filling pressure in argon at $P_{rf} \approx 75$ kW (two antennas).

to 45 ms, the plasma in the L mode is characterized by strong density and potential fluctuations. At the third step a spontaneous transition to the H mode occurs at about 50th ms of the discharge. The negative radial electric field [Fig. 5(c)] steps up in the L mode (reaching ~ 8 V/cm) prior to the transition, as does the ion temperature (not shown). After a few oscillations during the transition (from 46 to 53 ms), E_r eventually stabilizes in the H mode at a level of about 10 V/cm. It is important to note that in a wide range of experimental conditions the depth of the potential well in plasma, $\Delta V = V_p(a) - V_p(0)$, is well correlated with the ion temperature, so that $T_i/e\Delta V = (0.7-1.3)$.

The difference in the absolute value of the threshold rf power shown in Fig. 4 ($P_{rf} \approx 55$ kW) and in Fig. 5 ($P_{rf} \approx 80$ kW) is due to the different antenna geometries used.¹³ The rf power threshold for the transition is found to be lower when the power is launched using one antenna (as in Fig. 4) than in the case when two saddle loop antennas are used. The

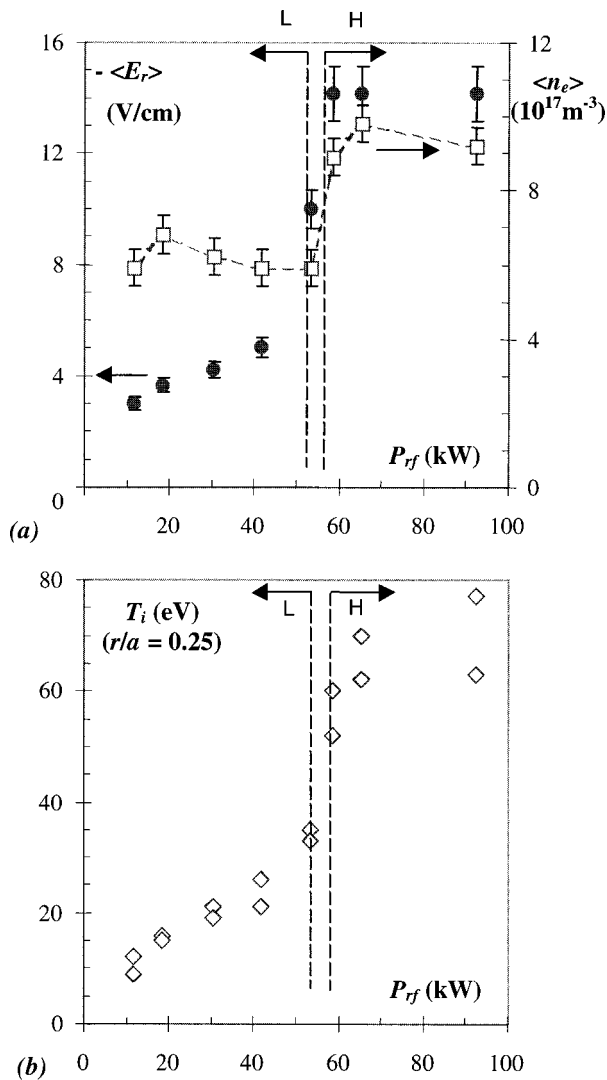


FIG. 4. Plasma parameters during the rf power scan (single antenna configuration) at $B=0.08$ T and $P_{\text{fill}}=3 \times 10^{-5}$ Torr in the magnetic configuration with $\iota \approx 1.41$: (a) line-average density (open squares) and the average radial electric field (solid circles); (b) ion temperature at $r/a=0.25$ (diamonds).

parameter dependencies remain similar for both antenna configurations.

The scenarios of the transitions to the H mode described above are quite typical for all the magnetic configurations studied, with one important exception: an increase in rf power does not always lead to the H mode. As an example, we now consider the so-called standard magnetic configuration (no current in the helical winding) characterized by a lower rotational transform of $\iota \approx 1.1$ and higher magnetic shear ($\Delta\iota/\iota \approx 6 \times 10^{-2}$). In this configuration the H mode is also observed at $B \geq B_{\text{cr}}$, with B_{cr} being higher than that in the $\iota \approx 1.41$ configuration, though the scenario is similar: the increase in B correlates with a gradual increase in E_r until the H mode is reached and E_r jumps to a more negative value. The rf power threshold conditions in this configuration appear to be drastically different from those shown in Figs. 4 and 5. At a fixed magnetic field and fixed gas filling pressure the H mode is reached when the rf power is reduced, as

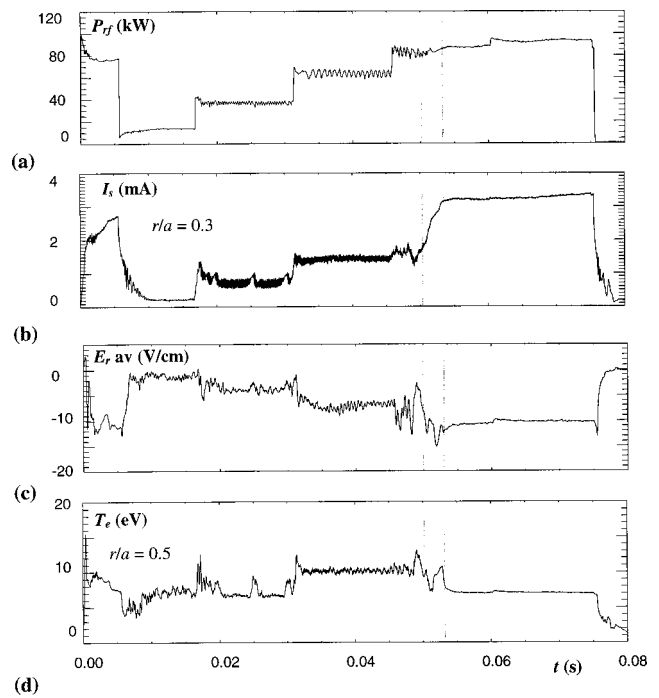


FIG. 5. Time evolution of the plasma parameters during the power step discharge in the magnetic configuration with $\iota \approx 1.41$ at $B=0.077$ T and $P_{\text{fill}}=1.7 \times 10^{-5}$ Torr. Two rf antennas.

shown in Fig. 6. But again, the H mode is reached (at ~ 20 kW of rf power) when the radial electric field increases up to about 10 V/cm with the decrease of the rf power. The transition is correlated with the fluctuation suppression (the squares in Fig. 6). This effect, namely, the reversed power threshold for the transition, is also observed during the rf power modulation experiment. Figure 7 shows the time evolution of the plasma parameters during a power step discharge in the standard magnetic configuration. In this case the H mode is reached at the first step (lowest power, from 19 to 32 ms). During the second power step, the electron density [actually the ion saturation current in Fig. 7(b)] is

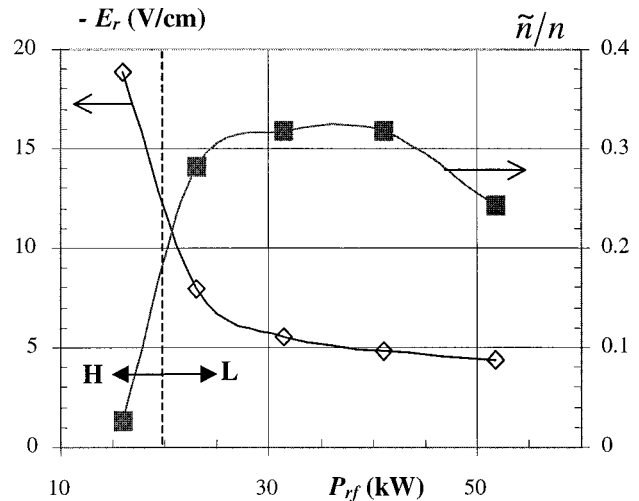


FIG. 6. The radial electric field (open diamonds) and the relative fluctuation level (solid squares) during the rf power scan in the standard magnetic configuration at $B=0.123$ T, $P_{\text{fill}}=3 \times 10^{-5}$ Torr in argon. Two rf antennas.

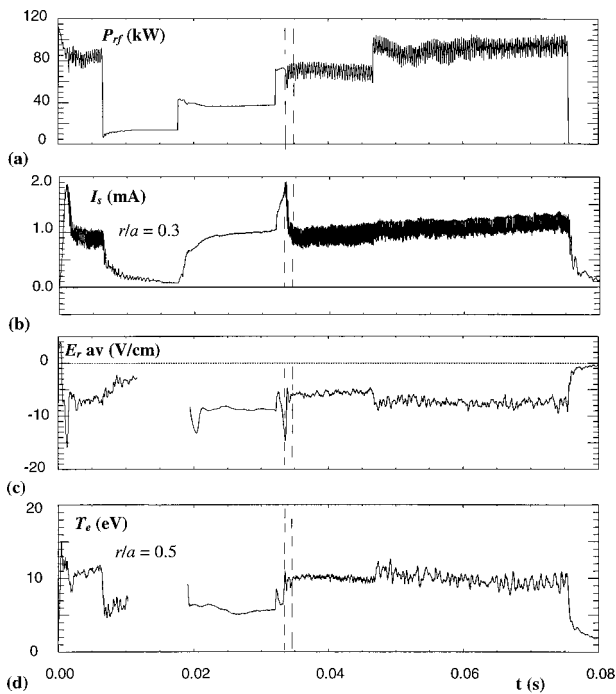


FIG. 7. Time evolution of the plasma parameters during the power step discharge in the standard magnetic configuration ($l \approx 1.1$) at $B = 0.12$ T and $P_{\text{fill}} = 9.6 \times 10^{-6}$ Torr. Two rf antennas.

trying to reach a new level, twice as high as during the first step, but then falls into the L mode at $t \approx 35$ ms. Such high to low confinement (H–L) transitions are typical for the standard magnetic configuration. The radial electric field decreases across the H–L transition from 10 to ~ 6 V/cm and then increases during the following power step in the L mode to about 8 V/cm, as shown in Fig. 7(c).

Summarizing these observations, regardless of the scenario, the transitions between the two modes of confinement are observed when the radial electric field reaches some critical value E_r^{crit} . The ways to drive $E_r (< 0)$ up to the transition include the following: an increase in the magnetic field, a decrease in the neutral filling pressure, and an *increase* or *decrease* in the rf power. At this point we postulate that driving E_r up to E_r^{crit} is a necessary condition for the confinement bifurcation. In the next section we consider the ion confinement in H-1, since understanding of the ion loss is critical for our further discussion on the formation of the radial electric field.

IV. ION ORBIT AND ION LOSS MODELING

A surprisingly high ion temperature observed in the H-1 heliac discharges at low magnetic fields⁹ raises a question about the details of the ion confinement and loss mechanisms. A combination of the three factors, namely, the high ion temperature (up to 200 eV), low magnetic field (< 0.1 T), and a high ion mass ($m_i = 40$ in argon or $m_i = 20$ in neon) brings the ion gyroradius to the order of magnitude of the minor plasma radius. This makes use of the theory and numerical modeling results¹⁴ based on the guiding center approximation invalid for the described experi-

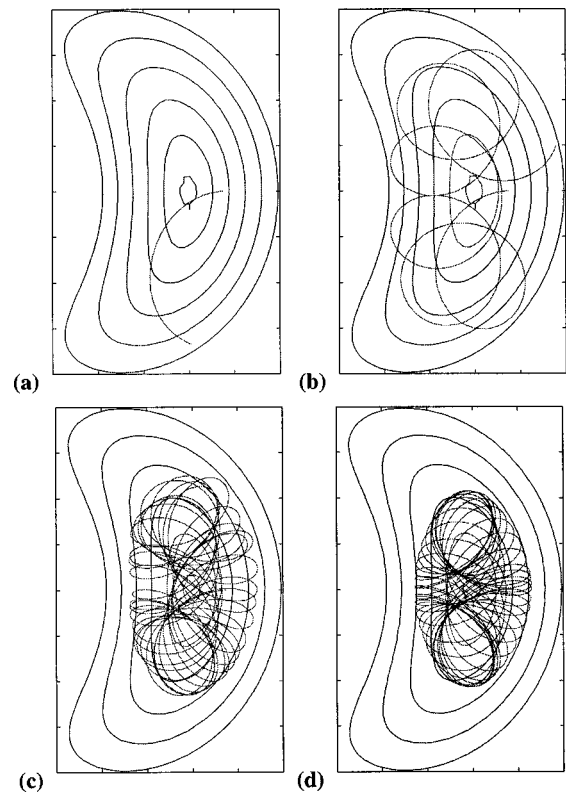


FIG. 8. Examples of the ion orbits: $T_i = 45$ eV, $B = 0.1$ T. The edge plasma potential $V_a = 0$ (a), $V_a = 15$ V (b), $V_a = 60$ V (c), and $V_a = 80$ (d).

ments and requires a study of exact ion orbits. In this section, we present the results on the ion trajectory modeling in the conditions very close to the plasma conditions described in Secs. II and III: singly charged argon ions at $B < 0.2$ T in the presence of the inward-directed radial electric field.

The ion orbits in the 3-D magnetic field of the H-1 heliac are followed by solving the Lorentz force equation $d\mathbf{V}/dt = (q/m_i)(\mathbf{V} \times \mathbf{B} + \mathbf{E})$ in real coordinates. A Gourdon code¹⁵ is used to produce the magnetic field $\mathbf{B}(r, \phi, z)$ and the flux surface coordinates $\rho(r, \phi, z)$ on a grid. The plasma potential profile is modeled to approximate the experimentally measured profile in the form $V_p = V_a \rho^2$, where V_a is the plasma potential at the edge and $0 \leq \rho \leq 1$. After defining the initial conditions, the ion orbits are followed using a standard adaptive step size Runge–Kutta integrator routine.

The examples of the individual trajectories are shown in Fig. 8. The trajectories are produced for ions with the energy of $T_i \approx 45$ eV at $B = 0.1$ T for a few values of the plasma potential V_a at the edge (central potential $V_0 = 0$). The orbits shown are the projections of the real coordinate orbits into a poloidal cross section of the flux surfaces. The particles are launched at $r/a = 0.3$ with the same initial conditions (velocity, pitch angle, and gyrophase). This figure illustrates an important role of the radial electric field in the ion confinement under the conditions when the electric force in the Lorentz force equation is comparable to the magnetic force. The radial electric field localizes the ion orbit, slightly improving the confinement of the weakly magnetized ions.

To study the ion loss, an ensemble averaging is performed. This includes averaging over the initial conditions of

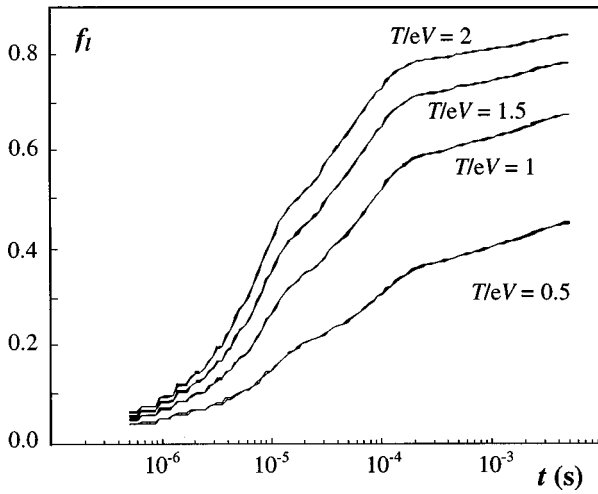


FIG. 9. The fraction of particles lost versus time from the start for different ion temperatures. The magnetic field is $B=0.1$ T and the edge plasma potential is $V_a=46$ V.

the monoenergetic particles. The poloidal and toroidal coordinates, as well as the particle pitch angle and gyrophase, are averaged randomly on a grid. The radial averaging uses a variable grid with a number of particles launched at the radius r_0 , $N(r_0)$, being a function of the approximated experimental density profile, $n(r)$: $N(r_0) = L \int_0^{r_0} n(r) r dr$, where $L \approx 2\pi R$ (R is the major radius). Typically about 3000 particles are used in the loss modeling for the fixed particle energy, the radial electric field, and the magnetic field. The results are averaged over the range of particle energies and are properly weighted to simulate the Maxwellian distribution with the temperature T .

The loss is defined as a rate at which particles leave the plasma. An ion is considered to be lost as soon as its orbit intersects the last closed flux surface (LCFS). Though there is a chance for a weakly magnetized ion to come back, the radial electric field, which has been found to be positive (repelling for ions) at $r/a > 1$,⁹ would push it farther away from the LCFS.

Figure 9 shows a fraction of ions (out of total number of particles) lost, f_l , as a function of time for different ratios T/eV_a of the equilibrium temperature to the edge potential. On the time scale of the ion collision time ($\tau_{in} \sim 3 \times 10^{-4}$ s) in this experiment and for typical $T/eV_a \sim 1$, more than 50% of particles are lost. The fraction of lost particles increases as the ion temperature grows.

We define an average loss current (or flux) as the value, which is proportional to $\Gamma_i^{orbit} \propto (V_p/S_p)n f_l / \tau_{cr}$, where V_p and S_p are the plasma volume and the surface area correspondingly, n is the particle density, and τ_{cr} is a characteristic time scale of the loss. Either we fix the observation time τ and measure the loss fraction f_l as a function of plasma parameters, or measure the time during which a fixed fraction of particles (e.g., 50%) is lost in direct losses. If we fix the loss fraction at, for example, $f_l=0.5$ and measure the average loss time τ_{cr} , we find that the loss rate and Γ_i^{orbit} is proportional to $(1/B^2)$.

Figure 10 shows the fraction of the particles lost during

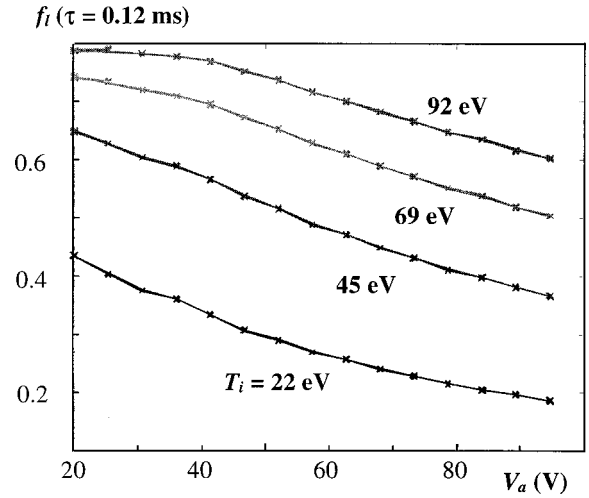


FIG. 10. The fraction of particles lost in 0.12 ms as a function of the plasma edge potential V_a for different ion temperatures. The magnetic field is $B=0.1$ T.

the first 0.12 ms after launch as a function of the edge potential V_a for different ion temperatures. This fraction decreases with the increase in the radial electric field. The decrease is relatively slow: the fraction of lost ions changes from about 65% with no radial electric field to only about 55% at $T_i/eV_a \sim 1$ (Fig. 10, $T_i=45$ eV). The decrease in Γ_i^{orbit} with the increase in E_r is due to some improvement in the ion orbits seen in Fig. 8. This orbit improvement of the weakly magnetized ions discussed here is not as dramatic as the orbit improvement of the neoclassical trapped ions at a higher magnetic field and smaller ion gyroradius.^{14,16} It has been shown in Ref. 14 that the collisionless ion loss fractions in the guiding center modeling in H-1 (hydrogen, $B=1.0$ T) decreases from about 40% when no radial electric field is present, down to zero at $T_i/eV_a \sim 1$.

Summarizing, the collisionless radial ion flux is proportional to the ion temperature T_i , and is a relatively weak decreasing function of the radial electric field, as shown in Fig. 10. The flux decreases as $(1/B^2)$ when both T_i and E_r are fixed.

V. QUALITATIVE MODEL OF THE RADIAL ELECTRIC FIELD FORMATION AND COMPARISON WITH EXPERIMENT

Once the scaling of the ion orbit loss is known from the numerical experiment of Sec. IV, we may build a qualitative model of the radial electric field formation. This field is generated by the radial currents (see, for example, Refs. 1, 17, and 18), and it can be shown using Poisson's equation that

$$\epsilon_0 \epsilon_{\perp} \frac{\partial}{\partial t} E_r = e(\Gamma_e - \Gamma_i), \quad (1)$$

where ϵ_{\perp} is the perpendicular dielectric constant. In steady state the electron and ion fluxes balance each other, so that the net radial current is zero, $\Gamma_e = \Gamma_i$.

As was shown in the previous section, the high-temperature ions in H-1 are confined by the combined effect of the magnetic and the radial electric fields. In the condi-

tions, typical for the described experiments, the ion orbit width is of the order of the plasma minor radius. The average lifetime of ions is shorter than the collision time τ_i and the direct particle losses exceeds 50% on a time scale of τ_i . Even at higher E_r , the direct orbit loss remains to be the dominant loss mechanism for ions. The electrons, in contrast, are strongly magnetized with the electron gyroradius being of the order of $\rho_e \approx 0.1$ mm. The electron collision rate is considerably higher than that of the ions and is of the order of $\nu_e \approx 6 \times 10^5$ 1/s. In these conditions the electrons are in the plateau regime, since the electron collisionality parameter $\nu_e^* = \nu_e L_{\parallel} / (\epsilon_h V_{Te})$ is about 0.5 (where L_{\parallel} is the parallel connection length, in H-1, $L_{\parallel} \approx 0.3$ m, $\epsilon_h \approx 0.5$, and $V_{Te} \approx 1.5 \times 10^6$ m/s is the electron thermal velocity). The electron losses include the neoclassical plus the fluctuation-induced flux. We assume that the fluctuation-induced transport is ambipolar, i.e., $\Gamma_e^{\text{fluct}} = \Gamma_i^{\text{fluct}}$. The quasineutrality condition would require the ion orbit loss to be balanced in steady state by the electron neoclassical (NC) flux: $\Gamma_e^{\text{NC}} = \Gamma_i^{\text{orbit}}$. For the plateau regime the neoclassical flux in the presence of the radial electric field is given by^{17,19}

$$\Gamma_e^{\text{NC}} = -n \frac{\pi^{1/2}}{2} \epsilon^2 \frac{\rho_e}{r} \frac{T_e}{e B_{\theta}} \left(\frac{1}{n} \frac{dn}{dr} + \frac{3}{2} \frac{1}{T_e} \frac{dT_e}{dr} - \frac{e}{T_e} (E_r - B_{\theta} U_{e\parallel}) \right) \exp \left[- \left(\frac{E_r}{B_{\theta} V_{Te}} \right)^2 \right], \quad (2)$$

or, since the exponential factor on the right-hand side of the equation (2) is about unity and the mean velocity along the magnetic field $U_{e\parallel}$ is small,⁹

$$\Gamma_e^{\text{NC}} \sim \frac{n T_e^{3/2}}{B^2} \left(\frac{1}{n} \frac{dn}{dr} + \frac{3}{2} \frac{1}{T_e} \frac{dT_e}{dr} - \frac{e E_r}{T_e} \right).$$

The direct ion orbit flux has a similar magnetic field scaling of $\sim (1/B^2)$. It is an increasing function of the ion temperature and a decreasing function of the radial electric field (Fig. 10) in the range of the experimental conditions described in Sec. III.

We propose the following scheme of the radial electric field formation. The rf heating scheme of the radial electric field formation. The rf heating mechanism by the helicon waves in H-1 is not quite clear,⁹ but it looks like it is capable of heating both electrons and ions depending on the plasma conditions. If ions are heated more efficiently than electrons, then the increase in rf power leads to a T_i increase and the ion orbit loss increases in the outer half of the plasma radius. This must be compensated for by an increase in the outward electron current to prevent the buildup of negative space charge. This can be graphically interpreted if we plot the electron and the ion fluxes discussed above versus the radial electric field, as shown in Fig. 11. The range of the plasma parameters is taken from the experiment. It should be noted that the first two terms on the right-hand side of the equation (2) nearly compensate for each other since T_e profiles are hollow and n_e profiles are peaked in H-1. The equilibrium radial electric field is defined as the intersection of $\Gamma_i(E_r)$ and $\Gamma_e(E_r)$ in Fig. 11. If the electron temperature is fixed, then the increase in the ion temperature leads to the increase

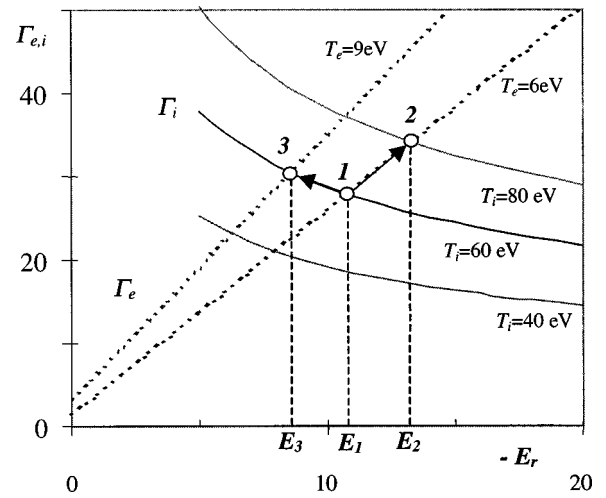


FIG. 11. The electron (dotted lines) and the ion (solid lines) radial fluxes versus the radial electric field for different electron and ion temperatures.

in E_r , (transition 1 \rightarrow 2 in Fig. 11). On the other hand, the increase in the T_e at constant T_i will bring the intersection point farther to the left, i.e., to lower E_r .

In the power scan and the power step experiments in the standard magnetic configuration, the decrease in E_r with the increase in P_{rf} (Figs. 6 and 7) can be attributed to a preferential electron heating in the inner regions of plasma. Indeed, the electron temperature at $r/a=0.5$ increases during the power step from 5 to 9 eV, as shown in Fig. 7(d). Figure 12 shows the expanded traces of T_e and E_r about the power step. The electron temperature increases right after the power step and *before* any significant changes in E_r .

A similar analysis of the discharge with the L-H transition (Fig. 5) shows that in this case the electron temperature does not change at all before the bifurcation. The expanded traces of T_e and E_r for this case are shown in Fig. 13.

Such behavior qualitatively agrees with the simple model presented above. The ion heating in the inner regions of plasma increases the radial electric field in any scenario of the approaches to the bifurcations: an increase in B (Fig. 1), decrease in P_{fill} (Fig. 2), or increases in P_{rf} (Fig. 3). In some cases, like in the standard magnetic configuration, the in-

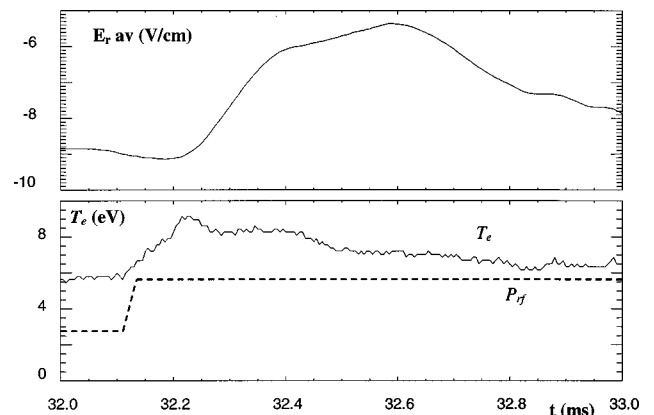


FIG. 12. Time evolution of the average radial electric field and the electron temperature at $r/a=0.5$ during the power step discharge shown in Fig. 7.

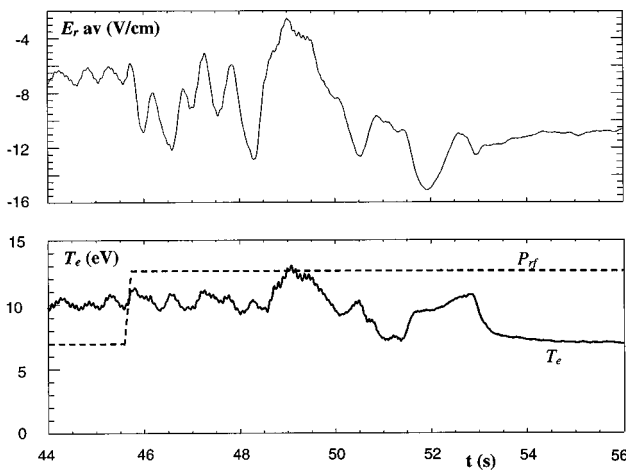


FIG. 13. Time evolution of the average radial electric field and the electron temperature at $r/a=0.5$ during the power step discharge shown in Fig. 5.

crease in the electron temperature (and corresponding increase in Γ_e) can compensate the increase in Γ_i or can even result in the lower equilibrium radial electric field (transition $1 \rightarrow 3$ in Fig. 11).

VI. SUMMARY AND DISCUSSION

The conditions and thresholds of the transitions between low and high confinement modes have been studied in the H-1 heliac. The factors affecting the thresholds include the following:

- (a) magnetic configuration;
- (b) magnetic field;
- (c) filling pressure of the working gas; and
- (d) radio-frequency power.

It is shown that transitions, either from low to high confinement (L–H), or from high to low (H–L), occur when the radial electric field is close to some critical value of $E_r^{\text{cr}} = (10\text{--}15 \text{ V/cm})$.

For the L–H transitions, the negative radial electric field increases monotonically in the L mode with the increase in the magnetic field (Fig. 2). The ion temperature also increases with B . A jump in E_r to an even more negative value in the H mode is correlated with the steepening of the ion pressure profile. The time scale of the radial electric field “bifurcation” is very close to the time scale of the modification in the density profile. We have not found any evidence that the radial electric field increases before the increase in the pressure gradient, though it typically oscillates during the transition.

Similarly, the radial electric field increases monotonically in the L mode before the transition with the increase in the rf power, as shown during the power scan in Fig. 4, or during the power step discharge in Fig. 5. Again, the increase in the radial electric field in these conditions is always pretty well correlated with the increase in the ion temperature at constant density (Fig. 4).

This seems to be consistent with a simple radial force balance argument. According to the radial force balance equation, $E_r = (z_i e n_i)^{-1} \nabla P_i - V_{\theta i} B_\phi + V_{\phi i} B_\theta$, where $z_i e$ is the ion charge, n_i is the ion density, P_i is the ion pressure,

$V_{\theta i}$ and $V_{\phi i}$ are the poloidal and toroidal rotation velocities, respectively, and B_θ and B_ϕ are the poloidal and toroidal components of the magnetic field. The radial electric field is balanced, in our case, by the ion pressure gradient (the first term in the right-hand side) since the bulk plasma velocities have been shown to be small compared with the $\mathbf{E} \times \mathbf{B}$ drift velocity.⁹ The increase in the radial electric field with the increase in B or P_{rf} can be attributed to the increase in either T_i or $(1/n)(dn/dr)$. The latter does not significantly change in the L mode, as shown in Fig. 2(b), so it is likely that the ion temperature is the major drive.

The dependence of the critical magnetic field on the gas filling pressure can also be interpreted in terms of the ion heating (or confinement) efficiency. At a fixed magnetic field, the ion temperature in the L mode decreases with the increase in the filling pressure (Fig. 3), as does the radial electric field. To compensate for this decrease in E_r with P_{fill} , the magnetic field should be brought up to increase the radial electric field to $E_r = E_r^{\text{cr}}$.

Oversimplifying, the radial electric field is a function of the ion temperature and the ion temperature is defined by the combination of effects of the magnetic field, rf power, and the filling pressure (neutral density).

In this simple picture we neglected the role of electrons in the radial electric field formation. This role is quite important, as shown in Sec. V. The increase in the electron temperature in the inner plasma region can lead to the decrease in the radial electric field and be responsible for the transition from high to low confinement, as observed in the standard magnetic configuration (Figs. 6–7, 12).

The details of the rf power deposition may also be essential for the interpretation of the difference in the power threshold in different antenna configurations (Figs. 4 and 5). The difference in the threshold power in this case may be due to the difference in the relative electron/ion heating when one or two antennas are used, even if the total absorbed power remains the same. Future studies of the mechanisms of plasma heating using helicon-type antennas could shed some light on the details of E_r formation in H-1. The role of the relative ion/electron heating in the formation of the radial electric field can also be studied in the future by using two different heating schemes, so that the heating of ions and electrons is decoupled (for example, by using the electron cyclotron resonance and the ion cyclotron resonance heating).

Summarizing, the transitions between low and high confinement modes in H-1 are observed, when the radial electric field reaches some critical level (between 10 and 15 V/cm). The electric field formation depends on the relative loss of the electrons and ions, which, in turn, depend on the electron and ion temperature. This radial electric field (or its gradient) suppresses the fluctuations and fluctuation-induced transport. This is followed by the improvement in confinement. The effect of the radial electric field on the fluctuations and associated transport will be reported in a separate paper.

ACKNOWLEDGMENTS

The authors would like to thank R. W. Boswell, J. H. Harris, and other members of the Plasma Research Labora-

tory for useful discussions. We also thank R. Davies, R. Kimlin, J. Wach, and G. C. J. Davies for the operational support.

- ¹K. Itoh and S.-I. Itoh, *Plasma Phys. Controlled Fusion* **38**, 1 (1996).
- ²K. H. Burrell, *Plasma Phys. Controlled Fusion* **36**, A291 (1994).
- ³F. Wagner, J. Baldzuhn, R. Brakel, R. Burhenn, V. Erckmann, T. Estrada, P. Grigull, J. H. Hartfuss, G. Herre, M. Hirsch, J. V. Hofmann, R. Jaenicke, A. Rudyj, U. Stroth, A. Weller, and the W7-AS Team, *Plasma Phys. Controlled Fusion* **36**, A61 (1994).
- ⁴K. Toi, S. Ohdachi, T. Morisaki, S. Sakakibara, S. Morita, T. Minami, K. Tanaka, H. Yamada, S. Okamura, K. Nishimura, K. Matsuoka, I. Yamada, R. Akiyama, A. Ando, A. Ejiri, K. Ida, H. Idei, H. Iguchi, A. Komori, S. Kubo, K. Narihara, T. Ozaki, C. Takahashi, K. Tsumori, and J. Xu, *Plasma Phys. Controlled Fusion* **38**, 1289 (1996).
- ⁵K. Ida, K. Kondo, K. Nagasaki, T. Hamada, S. Hidekuma, F. Sano, H. Zushi, T. Mizuuchi, H. Okada, S. Besshou, K. Watanabe, and T. Obiki, *Phys. Rev. Lett.* **76**, 1268 (1996).
- ⁶D. Craig, A. F. Almagri, J. K. Anderson, J. T. Chapman, C.-S. Chiang, N. A. Crocker, D. J. Den Hartog, G. Fiksel, S. C. Prager, J. S. Sarff, and M. R. Stoneking, *Phys. Rev. Lett.* **79**, 1865 (1997).
- ⁷O. Sakai, Y. Yasaka, and R. Itatani, *Phys. Rev. Lett.* **70**, 4071 (1993).
- ⁸M. G. Shats, D. L. Rudakov, B. D. Blackwell, G. G. Borg, R. L. Dewar, S. M. Hamberger, J. Howard, and L. E. Sharp, *Phys. Rev. Lett.* **77**, 4190 (1996).
- ⁹M. G. Shats, D. L. Rudakov, R. W. Boswell, and G. G. Borg, *Phys. Plasmas* **4**, 3629 (1997).
- ¹⁰M. G. Shats and D. L. Rudakov, *Phys. Rev. Lett.* **79**, 2690 (1997).
- ¹¹T. N. Carlstrom, *Plasma Phys. Controlled Fusion* **38**, 1149 (1996).
- ¹²S. M. Hamberger, B. D. Blackwell, L. E. Sharp, and D. B. Shenton, *Fusion Technol.* **17**, 123 (1990).
- ¹³G. G. Borg, B. D. Blackwell, S. M. Hamberger, D. Rudakov, D. A. Schneider, L. E. Sharp, M. Shats, and B. C. Zhang, *Fusion Eng. Des.* **26**, 191 (1995).
- ¹⁴S. L. Painter and H. G. Gardner, *Nucl. Fusion* **33**, 1107 (1993).
- ¹⁵C. Gourdon, D. Marty, E. K. Maschke, and J. Touche, *Nucl. Fusion* **11**, 161 (1971).
- ¹⁶E. R. Solano, J. A. Rome, and S. P. Hirshman, *Nucl. Fusion* **28**, 157 (1988).
- ¹⁷T. E. Stringer, *Nucl. Fusion* **33**, 1249 (1993).
- ¹⁸M. Coronado and J. N. Talmadge, *Phys. Fluids B* **5**, 1200 (1993).
- ¹⁹A. A. Galeev and R. Z. Sagdeev, *Sov. Phys. JETP* **26**, 233 (1968).